Theoretical Study of the Mechanism of Oxidative Addition of Allyl−Ammonium and −Iminium Salts to Low-Valent Metal Complexes. Rationalization of Selective C−N and N−H Bond Activation

Maricel Torrent,[†,‡] Djamaladdin G. Musaev,*[,‡] and Keiji Morokuma*[,‡]

Institute of Computational Chemistry and Department of Chemistry, University of Girona, Girona, Spain E-17071, and Cherry L. Emerson Center for Scientific Computation and Department of Chemistry, Emory University, Atlanta, Georgia 30322

Received June 2, 2000

A theoretical study has been carried out for the mechanism of the reactions of allylammonium and -iminium substrates with Ni(0) complexes using the B3LYP density functional method. The main findings are as follows: (1) The actual active catalyst in the oxidative addition of ammonium and iminium salts is the bisphosphine−nickel complex. (2) For allylammonium salts the reaction is found to proceed via an *associative* mechanism (rather than a dissociative path) which involves (i) coordination of the allylammonium cation to the active metal catalyst, (ii) oxidative addition of the C−N bond to the Ni(0) complex, (iii) coordination of NH_3 to yield a pentacoordinated intermediate, and (iv) loss of a phosphine ligand. The analogous reaction involving allyliminium salts does not follow the same mechanistic pattern; once the allyliminium cation is coordinated to the metal, the reaction prefers to proceed in a *dissociative* fashion. This preference is likely to be enhanced in solution. (3) The main difference between allylammonium and -iminium reaction mechanisms lies in the relative barriers corresponding to the insertion of the catalyst into the C−N bond leading to the pentacoordinated intermediate. For allylammonium cations, such a step is calculated to be less energy demanding than phosphine loss, whereas for allyliminium, the situation is reversed. (4) Finally the observed preference of allyliminium substrates to undergo C−N cleavage rather than N−H cleavage has been also investigated. The reason that allyl salt does not yield hydrido complexes is the kinetic impairment found for the N−H bond cleavage as compared to C−N. Intramolecular N−H activation is not allowed because of the high barriers corresponding to the three-centered transition states involved in the reaction. The structural rearrangements required for the coordinated iminium to form an η^2-NH complex make the process prohibitive.

I. Introduction

Transition-metal-promoted C−N bond activation[1] is a major step in several catalytic processes.[2] In the past few years, it has been reported[3] that Pt and Ru compounds promote the cleavage of the allyl−N bond of allylamines with subsequent transfer of the allyl group to the metal center. Very recently it has also been possible to rupture the C−N single bond of aniline[4] and anionic amides[5] (and to afford ring-opening of pyridine[6] and pyrrole[7] rings as well) by using highly reactive trivalent group 5 metals (Nb and Ta). Schrock and coworkers have reported on multiple C−N bond activation via the formation of nitrido complexes by metathesis of W≡W triple bonds with nitriles.[8] Other examples are the four-electron oxidative addition of isocyanates, carbodiimides, and imine C=N double bonds to Mo(II) or W(II) phosphine complexes to give Mo(VI)− or W(VI)−imido compounds[9] and the nucleophile-induced cleavage of a C−N bond of an η^2-(C,N)-coordinated pyridine ring.[10]

To the best of our knowledge, the activation of a C−N bond by Ni systems has been reported only twice in the literature. In a pioneering study, Chan et al.[11] reported

[†] University of Girona.
[‡] Emory University.

(1) (a) Hagadorn, J. R.; Arnold, J. *Organometallics* **1994**, *13*, 4670. (b) Poszmik, G.; Carroll, P. J.; Wayland, B. B. *Organometallics* **1993**, *12*, 3410. (c) Adams, R. D.; Chen, G. *Organometallics* **1993**, *12*, 2070.

(2) (a) Roberto, D.; Alper, H. *J. Am. Chem. Soc.* **1989**, *111*, 7539. (b) Laine, R. M.; Thomas, D. W.; Cary, L. W. *J. Am. Chem. Soc.* **1982**, *104*, 1763. (c) Roundhill, D. M. *Chem. Rev.* **1992**, *92*, 1.

(3) (a) Hiraki, K.; Matsunaga, T. *Organometallics* **1994**, *13*, 1878. (b) Nagashima, H.; Katsunori, M.; Shiota, Y.; Ara, K.; Itoh, K.; Suzuki, H.; Oshima, N.; Moro-oka, Y. *Organometallics* **1985**, *4*, 1314. (c) Kurosawa, H. *Inorg. Chem.* **1976**, *15*, 120.

(4) Bonanno, J. B.; Henry, T. P.; Neithamer, D. R.; Wolczanski, P. T.; Lobkovsky, E. B. *J. Am. Chem. Soc.* **1996**, *118*, 5132.

(5) (a) Tayebani, M.; Feghali, K.; Gambarotta, S.; Bensimon, C. *Organometallics* **1997**, *16*, 5084. (b) Tayebani, M.; Gambarotta, S.; Yap, G. *Organometallics* **1998**, *17*, 3639.

(6) Kleckley, T. S.; Bennett, J. L.; Wolczanski, P. T.; Lobkovsky, E. B. *J. Am. Chem. Soc.* **1997**, *119*, 247.

(7) Tayebani, M.; Gambarotta, S.; Yap, G. P. A. *Angew. Chem., Int. Ed.* **1998**, *37*, 3002.

(8) Schrock, R. R.; Listemann, M. L.; Sturgeoff, L. G. *J. Am. Chem. Soc.* **1982**, *104*, 4293.

(9) (a) Hall, K. A.; Mayer, J. M. *J. Am. Chem. Soc.* **1992**, *114*, 10402. (b) Bryan, J. C.; Mayer, J. M. *J. Am. Chem. Soc.* **1990**, *112*, 2298.

(10) Weller, K. J.; Gray, S. D.; Briggs, P. M.; Wigley, D. E. *Organometallics* **1995**, *14*, 5588.

10.1021/om000468a CCC: $19.00
Publication on Web 09/20/2000

Scheme 1. Reported Reactions of Ammonium and Iminium Salts toward Ni(0)−Tertiary Phosphine Complexes (Cy = cyclohexyl)

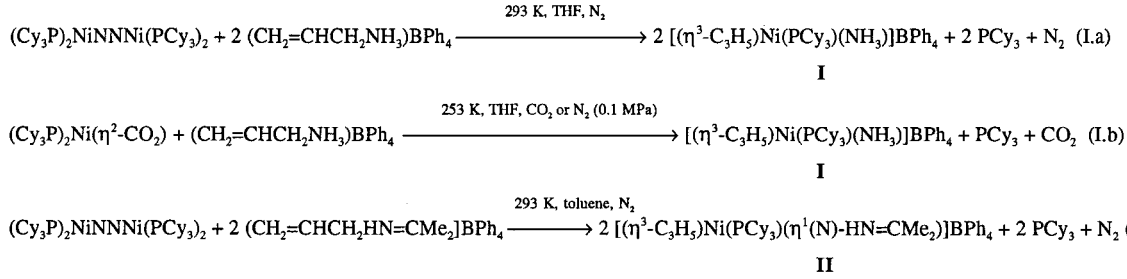

first the C−N bond cleavage of an N,N′-bridged porphyrin by different low-valent metal systems (such as $Fe_3(CO)_{12}$, $Ru_3(CO)_{12}$, and $Ni(CO)_4$) under severe conditions. A second paper has been published only recently by Aresta et al.;[12] it is the focus of our present theoretical study. Experimentally these authors showed that Ni(0) complexes can promote the activation of a C−N bond under very mild conditions and easily generate Ni systems with interesting catalytic properties.[12] In particular, it was reported that allylammonium and -iminium salts can add oxidatively to Ni(0)−phosphine complexes. This novel route (Scheme 1) represents a powerful way to the direct synthesis of cationic allyl−nickel systems, which are of considerable current interest because of their catalytic activity for reactions involving either olefins or dienes.[13,14] Until recently, such complexes were generally prepared in two steps via halide abstraction from neutral π-allyl systems[13,15] or by using methods that involve allyl group transfer from an oxygen or sulfur atom to nickel.[16,17]

Therefore the reactions in Scheme 1 constitute a new route to obtain ionic π-allyl−Ni complexes using stable, readily available, and very reactive allylammonium or -iminium salts.[12] Also, such reactions allow the synthesis of unprecedented asymmetric cationic π-allyl complexes bearing P- and N-ligands in the coordination sphere of nickel. However, despite the obvious advantages of the novel route, these experiments left unsolved several questions, including the following: (i) What are the structures and energetics of the assumed intermediates and transition states (TSs) involved in the reactions? (ii) Why do allylammonium and -iminium salts undergo N−C bond scission but not N−H bond scission? (iii) Are there any differences between the reactivity pattern of allylammonium and allyliminium substrates? In understanding these questions, quantum chemical calculations can be extremely useful. Therefore in the present paper we study, first, the potential energy surfaces (PES) and mechanisms of the reactions

$$Ni(PH_3)_2 + (CH_2{=}CHCH_2NH_3)^+ \rightarrow [(\eta^3\text{-}C_3H_5)Ni(PH_3)(NH_3)]^+,\ \mathbf{1},\ +\ PH_3 \quad (1)$$

$$Ni(PH_3)_2 + (CH_2{=}CHCH_2HN{=}CH_2)^+ \rightarrow [(\eta^3\text{-}C_3H_5)Ni(PH_3)(\eta^1(N)\text{-}HN{=}CH_2)]^+,\ \mathbf{2},\ +\ PH_3 \quad (2)$$

using the density functional method. Here reactions 1 and 2 are the models for the experimentally observed reactions I and II in Scheme 1, respectively. In the present paper, only the cationic part of the real salts is considered. In addition, the experimentally used CMe_2 and PCy_3 ligands are modeled here by CH_2 and PH_3, respectively, unless otherwise indicated. The question whether allylammonium and -iminium compounds have a common mechanistic pattern or their reactions involve different mechanisms will be addressed by comparing reactions 1 and 2 above.

Second, note that under experimental conditions, the only observed process during the reaction of Ni(0) complex with the allyliminium tetraphenylborate salt was the transfer of the allyl group from N to Ni (which corresponds to the C−N bond activation).[12] No products derived from N−H bond activation were formed (unless the allyl group is exchanged by an aromatic group).[12] To rationalize why C−N but not N−H activation takes place during reaction 2, the following pair of reactions will also be investigated here:

$$Ni(PH_3)_2 + (CH_2{=}CHCH_2HN{=}CH_2)^+ \rightarrow [\textit{trans}\text{-}(H)Ni(PH_3)_2(\eta^1(N)\text{-}CH_2{=}CHCH_2N{=}CH_2)]^+,\ \mathbf{3}\textit{-trans} \quad (3\text{-t})$$

$$Ni(PH_3)_2 + (CH_2{=}CHCH_2HN{=}CH_2)^+ \rightarrow [\textit{cis}\text{-}(H)Ni(PH_3)_2(\eta^1(N)\text{-}CH_2{=}CHCH_2N{=}CH_2)]^+,\ \mathbf{3}\textit{-cis} \quad (3\text{-c})$$

The present paper is organized as follows. In section II, we briefly describe the computational procedure used in this work. The calculated results are discussed in section III. A set of conclusions is drawn in section IV.

II. Computational Details

Unless otherwise indicated, geometries of all the stationary points on the PES of the above-mentioned reactions were optimized using the B3LYP hybrid functional,[18] which has been shown to predict reliable geometries and energetics for similar transition-metal−phosphine complexes.[19] Basis set I (denoted below as BSI), used for geometry optimization,

(11) Chan, Y. W.; Renner, M. W.; Balch, A. L. *Organometallics* **1983**, *2*, 1888.
(12) Aresta, M.; Quaranta, E.; Dibenedetto, A.; Giannoccaro, P.; Tommasi, I.; Lanfranchi, M.; Tiripicchio, A. *Organometallics* **1997**, *16*, 834.
(13) (a) Wilke, G. *Angew. Chem., Int. Ed. Engl.* **1988**, *27*, 185. (b) Keim, W. *Angew. Chem., Int. Ed. Engl.* **1990**, *29*, 235. (c) Tolman, C. A. *J. Am. Chem. Soc.* **1970**, *92*, 6777. (d) Commereuc, D.; Chauvin, Y. *Bull. Soc. Chim. Fr.* **1974**, 652.
(14) (a) Tobisch, S.; Bögel, H.; Taube, R. *Organometallics* **1996**, *15*, 3563. (b) Tobisch, S.; Bögel, H.; Taube, R. *Organometallics* **1998**, *17*, 1177.
(15) Jolly, P. W.; Wilke, G. *The Organic Chemistry of Nickel*; Academic Press: New York, 1974.
(16) (a) Castro, B.; Neibecker, D. *J. Organomet. Chem.* **1975**, *85*, C39. (b) Castro, B.; Neibecker, D. *J. Organomet. Chem.* **1977**, *134*, 105.
(17) Castro, B.; Neibecker, D. *Tetrahedron Lett.* **1977**, *27*, 2351.

Table 1. Binding Energies (BE) in kcal mol^{-1} for $(R_3P)_2Ni(CO_2)$ (R = H, CH_3)

system	BE(BSI)	BE(BSII)	BE(BSI) with ZPE	BE(BSII) with ZPE	BE(BSII) Gibbs FE[a]
		R = H			
$(H_3P)_2Ni(CO_2)$	0.0	0.0	0.0	0.0	0.0
$(H_3P)Ni(CO_2) + PH_3$	16.1	14.8	14.4	13.1	5.6
$Ni(PH_3)_2 + CO_2$	23.4	5.5	22.5	4.6	−3.3
		R = CH_3			
$[(CH_3)_3P]_2Ni(CO_2)$	0.0	0.0	0.0	0.0	0.0
$[(CH_3)_3P]Ni(CO_2) + P(CH_3)_3$	24.7	26.0	23.0	24.3	12.3
$Ni[P(CH_3)_3]_2 + CO_2$	18.1	5.4	16.0	3.3	−6.7

[a] Gibbs free energy at 1 atm, 298.15 K.

Table 2. Total Energies (in au, in italics) of Reference Systems and Relative Energies (in kcal mol^{-1}), Relative to Complex 1a, of Intermediates and Transition States for Reaction 1

compound	*E*(BSI)	*E*(BSII)	*E*(BSI) with ZPE	*E*(BSII) with ZPE	*G*(BSII)[a]
$(CH_2{=}CHCH_2NH_3)^+$	*−173.59542*	*−173.62931*	*−173.48183*	*−173.51572*	*−173.54333*
$Ni(PH_3)_2$	*−177.52072*	*−1851.08959*	*−177.46925*	*−1851.03812*	*−1851.06940*
PH_3	*−8.26987*	*−343.14432*	*−8.246586*	*−343.12104*	*−343.14109*
NH_3	*−56.54828*	*−56.55149*	*−56.514368*	*−56.517578*	*−56.53676*
1a	*−359.51061*	*−2368.27351*	*−359.34394*	*−2368.10683*	*−2368.14759*
path **A**					
1a	0.0	0.0	0.0	0.0	0.0
1b + PH_3	22.3	24.1	20.2	22.0	11.5
TS(1b→1c) + PH_3	35.1	37.9	30.0	32.8	22.1
1c + NH_3 + PH_3	33.9	35.6	26.3	28.0	8.1
1 + PH_3	−14.1	−15.2	−17.7	−18.8	−27.5
path **B**					
TS(1a→1d)	11.6	13.6	8.5	10.5	9.7
1d + NH_3	−1.5	2.5	−6.4	−2.4	−12.4
1e	−11.8	−11.5	−14.5	−14.2	−14.7
TS(1e→1)	−11.1	−9.7	−14.2	−12.8	−12.5

[a] Gibbs free energy at 1 atm, 298.15 K.

includes a standard double-ζ quality basis set, which consists of a lanl2dz basis set associated with the relativistic effective core potential (ECP)[20] for Ni and nonrelativistic ECP[21] for P, and D95 for the other atoms.[22] Basis set II (denoted below as BSII) was used for recalculation of the energetics at the B3LYP/BSI optimized geometries. For the Ni atom it corresponds to the basis set described by Wachters[23] (contraction Scheme 1 in the original paper[23]) augmented with one d (α = 0.1316) and one f (α = 2.3) polarization function, while for H, C, O, N, and P atoms it uses the standard 6-31G** basis set.[24] The nature of the calculated intermediates and TSs has been analyzed by doing normal-mode analysis at the B3LYP/BSI level. In Tables 1−5 we present energetics of the reactants, intermediates, TSs, and products of the reactions 1−3 at all levels of theory used in this paper; however, we mainly discuss the B3LYP/BSII values of those including zero-point-energy (B3LYP/BSII + ZPE) and/or entropy (Gibbs free energies at 1 atm, 298.15 K) corrections. Note that ZPE and entropy corrections are calculated at the B3LYP/BSI level and added to the B3LYP/BSII total energies.

Calculations were performed with the Gaussian-94 package,[25] supplemented by our ECP analytical second-derivative code.[26] Solvation effects were analyzed for a selected set of molecules by means of reaction field calculations using the polarizable dielectric model of Tomasi and co-workers.[27] Two-layered ONIOM calculations for a selected set of molecules (see further details in section III.B) were carried out with the Gaussian-98 package.[28]

III. Results and Discussion

Prior to dealing with the reactions presented in the Introduction, first we briefly evaluate the model used for the active catalyst (subsection A). The main goals of the paper, namely, allylammonium versus allylimin-

(18) (a) Becke, A. D. *Phys. Rev. A* **1988**, *38*, 3098. (b) Lee, C.; Yang, W.; Parr, R. G. *Phys. Rev. B* **1988**, *37*, 785. (c) Becke, A. D. *J. Chem. Phys.* **1993**, *98*, 5648.

(19) Cui, Q.; Musaev, D. G.; Morokuma, K. *Organometallics* **1997**, *16*, 1355.

(20) Hay, P. J.; Wadt, W. R. *J. Chem. Phys.* **1985**, *82*, 299.

(21) Wadt, W. R.; Hay, P. J. *J. Chem. Phys.* **1985**, *82*, 284.

(22) (a) Dunning, T. M., Jr. *J. Chem. Phys.* **1971**, *55*, 716. (b) Dunning, T. M., Jr. *J. Chem. Phys.* **1970**, *53*, 2823.

(23) Wachters, A. J. H. *J. Chem. Phys.* **1970**, *52*, 1033.

(24) (a) Ditchfield, R.; Hehre, W. J.; Pople, J. A. *J. Chem. Phys.* **1971**, *54*, 724. (b) Hehre, W. J.; Ditchfield, R.; Pople, J. A. *J. Chem. Phys.* **1972**, *56*, 2257. (c) Hariharan, P. C.; Pople, J. A. *Mol. Phys.* **1974**, *27*, 209. (d) Gordon, M. S. *Chem. Phys. Lett.* **1980**, *76*, 163. (e) Hariharan, P. C.; Pople, J. A. *Theor. Chim. Acta* **1973**, *28*, 213. (f) Frisch, M. J.; Pople, J. A.; Binkley, J. S. *J. Chem. Phys.* **1984**, *80*, 3265.

(25) Frisch, M. J.; Trucks, G. W.; Schlegel, H. B.; Gill, P. M. W.; Johnson, B. G.; Robb, M. A.; Cheesemen, J. R.; Keith, T. A.; Petersson, J. A.; Montgomery, J. A.; Raghavachari, K.; Al-Laham, M. A.; Zakrzewski, V. G.; Ortiz, J. V.; Foresman, J. B.; Cioslowski, J.; Stefanov, B. B.; Nanayakkara, A.; Challacombe, M.; Peng, C. Y.; Ayala, P. Y.; Chen, W.; Wong, M. W.; Andres, J. L.; Replogle, E. S.; Gomperts, R.; Martin, R. L.; Fox, D. J.; Binkley, J. S.; DeFrees, D. J.; Baker, J.; Stewart, J. J. P.; Head-Gordon, M.; Gonzales, C.; Pople, J. A. *Gaussian 94*; Gaussian Inc.: Pittsburgh, PA, 1995.

(26) Cui, Q.; Musaev, D. G.; Svensson, M.; Morokuma, K. *J. Phys. Chem.* **1996**, *100*, 10936.

(27) (a) Miertus, S.; Scrocco, E.; Tomasi, J. *Chem. Phys.* **1981**, *55*, 117. (b) Miertus, S.; Tomasi, J. *Chem. Phys.* **1982**, *65*, 239. (c) Cossi, M.; Barone, R.; Cammi, R.; Tomasi, J. *Chem. Phys. Lett.* **1996**, *255*, 327.

(28) Frisch, M. J.; Trucks, G. W.; Schlegel, H. B.; Scuseria, G. E.; Robb, M. A.; Cheeseman, J. R.; Zakrzewski, V. G.; Montgomery, J. A., Jr.; Stratmann, R. E.; Burant, J. C.; Dapprich, S.; Millam, J. M.; Daniels, A. D.; Kudin, K. N.; Strain, M. C.; Farkas, O.; Tomasi, J.; Barone, V.; Cossi, M.; Cammi, R.; Mennucci, B.; Pomelli, C.; Adamo, C.; Clifford, S.; Ochterski, J.; Petersson, G. A.; Ayala, P. Y.; Cui, Q.; Morokuma, K.; Malick, D. K.; Rabuck, A. D.; Raghavachari, K.; Foresman, J. B.; Cioslowski, J.; Ortiz, J. V.; Stefanov, B. B.; Liu, G.; Liashenko, A.; Piskorz, P.; Komaromi, I.; Gomperts, R.; Martin, R. L.; Fox, D. J.; Keith, T.; Al-Laham, M. A.; Peng, C. Y.; Nanayakkara, A.; Gonzalez, C.; Challacombe, M.; Gill, P. M. W.; Johnson, B.; Chen, W.; Wong, M. W.; Andres, J. L.; Gonzalez, C.; Head-Gordon, M.; Replogle, E. S.; Pople, J. A. *Gaussian 98, Revision A.1*; Gaussian, Inc.: Pittsburgh, PA, 1998.

Table 3. Total Energies (in au, in italics) of Reference Systems and Relative Energies (in kcal mol^{-1}), Relative to Complex 2a, of Intermediates and Transition States for Reaction 2

compound	*E*(BSI)	*E*(BSII)	*E*(BSI) with ZPE	*E*(BSII) with ZPE	*G*(BSII)[a]
$(CH_2{=}CHCH_2HN{=}CH_2)^+$	*−211.66601*	*−211.71101*	*−211.54907*	*−211.71101*	*−211.62333*
2a	*−397.61808*	*−2406.38421*	*−397.44690*	*−2406.38421*	*−2406.25622*
path **A**					
2a	0.0	0.0	0.0	0.0	0.0
TS(2a→2b)	27.4	27.5	26.4	26.5	21.8
2b + PH_3	26.9	26.6	24.4	24.1	14.9
TS(2b→2) + PH_3	56.6	52.9	52.0	48.3	41.2
2 + PH_3	12.3	5.0	8.4	1.1	−8.0
Path **B**					
TS$_C$−N from **2a**	45.7	42.1	42.4	38.8	39.4
TS(2a→2a′)	27.9	25.5	26.3	23.9	24.5
2a′	24.0	20.0	23.2	19.2	19.8
TS(2a′→2c)	41.2	37.5	37.7	34.0	31.5
2c + $HNCH_2$	27.9	21.3	23.9	17.3	7.1
2d	16.6	12.0	13.5	8.9	10.4
TS(2d→2e)	16.8	12.8	13.6	9.6	11.2
2e	3.6	4.7	0.8	1.9	−0.5
from path **A** to path **B**					
TS(2b→2a′)	37.2	37.4	35.0	35.2	39.9

[a] Gibbs free energy at 1 atm, 298.15 K.

Table 4. Reaction Enthalpies and Gibbs Free Energies (in kcal mol^{-1}) for Reactions 2, 3-c, and 3-t Relative to the Separated Reactants, $Ni(PH_3)_2$ + $[(CH_2{=}CHCH_2)HN{=}CH_2)]^+$

reaction	Δ*H*(BSI)	Δ*H*(BSII)	Δ*H*(BSI) with ZPE	Δ*H*(BSII) with ZPE	Δ*G*(BSII)[a]
2	−56.3	−45.8	−58.4	−47.9	−46.2
3-c	−45.2	−34.3	−46.5	−35.6	−23.0
3-t	−48.4	−40.0	−49.1	−40.7	−29.1

[a] Gibbs free energy at 1 atm, 298.15 K.

Table 5. Relative Energies (in kcal mol^{-1}), Relative to Complex 3a, of Intermediates and Transition States for Reactions 3-c and 3-t)

compound	*E*(BSI)	*E*(BSII)	*E*(BSI) with ZPE	*E*(BSII) with ZPE	*G*(BSII)[a]
3a	0.0	0.0	0.0	0.0	0.0
TS(3a→3-*cis*)	48.6	48.6	44.7	44.7	43.9
3-*cis*	23.4	21.7	20.4	18.7	18.4
3b + PH_3	26.7	27.6	24.5	25.4	15.8
TS(3b→3c) + PH_3	68.3	68.8	61.5	62.0	51.8
3c + PH_3	37.7	33.8	32.8	28.9	20.4
3-*trans*	19.7	16.1	17.2	13.6	14.3

[a] Gibbs free energy at 1 atm, 298.15 K.

ium, and C−N versus N−H bond activation, are discussed in subsections B and C, respectively.

A. Choice of the Model Active Catalyst. According to Scheme 1, two different Ni complexes were used as prereactant complex in the experiments by Aresta et al.:[12] bis[bis(tricyclohexylphosphine)nickel]dinitrogen, $[(PCy_3)_2Ni]_2N_2$, **a**, and [bis(tricyclohexylphosphine)(η^2-carbon dioxide)]nickel, $(Cy_3P)_2Ni(\eta^2\text{-}CO_2)$, **b**. As we discuss below, in both cases only the $Ni(PR_3)_2$ fragment is expected to participate actively in the bond activation process. Neither N_2 nor CO_2 is likely to play a significant role. Species **a** has been the first Ni(0) complex containing molecular nitrogen as ligand ever reported in the literature.[29] Interestingly, it was found that the nitrogen molecule in this species is bonded only weakly, and when a stream of argon gas is passed through a solution of the complex in toluene, N_2 is released with formation of $Ni(PCy_3)_2$.[29] These results suggest that a similar dissociation can be assumed to occur under the conditions of the reactions investigated here, leaving the bisphosphine−Ni complex as the active catalyst.

To check the validity of this assumption, we have calculated the Ni−N_2 binding energies of the model for species **a**, $[(PH_3)_2Ni]_2N_2$, using the B3LYP/BSI optimized geometries of the complexes given in Figure 1. As seen from this figure, $[(PH_3)_2Ni]_2N_2$ is a double end-on complex, with the N−N distance stretched by 0.035

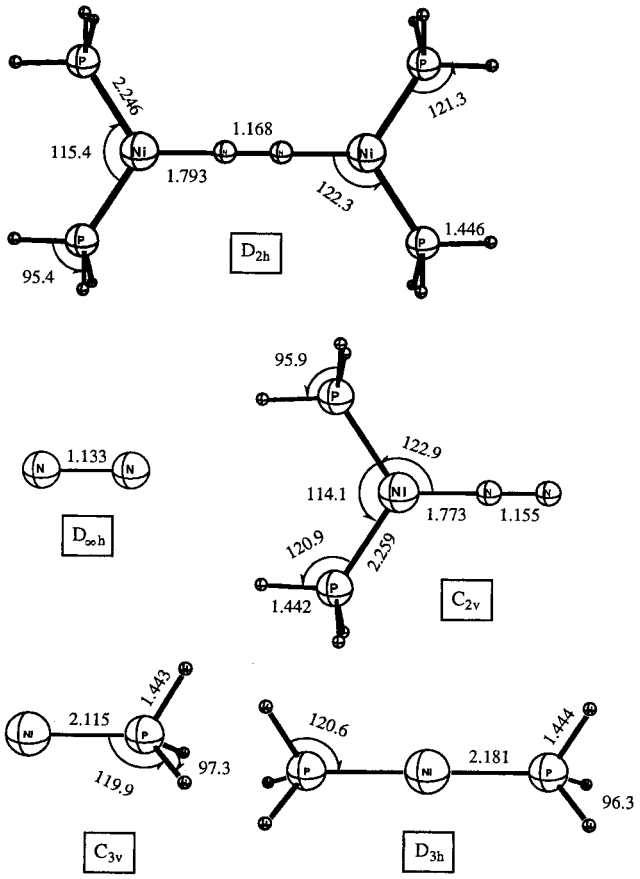

Figure 1. Selected geometrical parameters (distances, Å; angles, deg) of stationary points on the potential energy surface of the reactions $(NNiL_2)_2 \rightarrow NiL_2 + N_2NiL_2$ and N_2-$NiL_2 \rightarrow NiL_2 + N_2$ where L = PH_3.

(29) Jolly, P. W.; Jonas, K. *Angew. Chem.* **1968**, *80*, 705; *Angew. Chem., Int. Ed. Engl.* **1968**, *7*, 731.

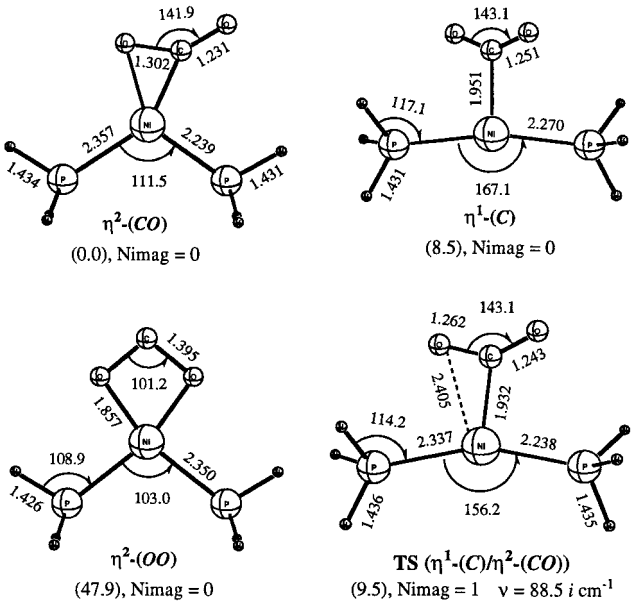

Figure 2. Selected geometrical parameters (distances, Å; angles, deg) of three different isomers of the $(H_3P)_2Ni(CO_2)$ catalyst, together with the TS connecting the two more stable isomers. Gibbs free energies (in parentheses) are in kcal mol^{-1}.

Å from free N_2, suggesting that the N−N bond here is midway between double and triple bond. Also, in the complex $(PH_3)_2NiN_2$, which results from the dissociation of one of the $Ni(PR_3)_2$ groups, N_2 coordinates in an end-on manner. The side-on complex is not energetically favorable and rearranges spontaneously to the end-on structure $(PH_3)_2Ni{-}NN$. The N−N distance in this C_{2v} intermediate is only slightly longer than that in free N_2, indicating that the N≡N triple bond is not broken. Once N_2 is released, the bent P−Ni−P skeleton in $(PH_3)_2NiN_2$ (114.1°) becomes linear in $Ni(PH_3)_2$. We will discuss the flexibility of the P−Ni−P bending later on. The computed B3LYP/BSII bond dissociation energies for $[(PH_3)_2Ni]_2N_2 \rightarrow [(PH_3)_2Ni]N_2 + Ni(PH_3)_2$ and $[(PH_3)_2Ni]N_2 \rightarrow Ni(PH_3)_2 + N_2$ are, respectively, 22.5 (10.8) kcal mol^{-1} and 28.1 (16.9) kcal mol^{-1} (here and below, with ZPE, and in parentheses, the Gibbs free energy).

On the other hand, the reactant catalyst $(Cy_3P)_2Ni(\eta^2\text{-}CO_2)$, **b**, may have three different isomers, as shown in Figure 2 for our model $(H_3P)_2Ni(CO_2)$. The most stable conformation is the η^2-(CO) structure, where CO_2 is coordinated to the metal center by its C atom and one of the O atoms, $(H_3P)_2Ni(\eta^2\text{-}CO_2)$. The optimized structure of this conformer is in good agreement with recent experiment, in which the solid-state structure of $Ni(PCy_3)_2(CO)_2$ involves the nickel atom lying in a square-planar environment defined by the two phosphorus atoms, the carbon atom, and one of the oxygen atoms. The η^1-(C) isomer of $(H_3P)_2Ni(\eta^1\text{-}CO_2)$ is found to be 9.3 (8.5) kcal mol^{-1} higher in energy than the η^2-(CO_2) structure and separated from it by a barrier of only 0.5 (1.0) kcal mol^{-1}. The **TS(η^1-(*C*)/η^2(*CO*))** responsible for this barrier has only one imaginary frequency ($\nu = 88.5i$ cm^{-1}) corresponding to the rotation of the CO_2 ligand, needed for CO_2 to become coplanar with P−Ni−P, as it is in the η^2-coordinated isomer. The third isomer with an η^2-O coordination involving the two O atoms of CO_2, $(H_3P)_2Ni(\eta^2(OO)\text{-}CO_2)$, is found to be a very unstable structure, lying 47.9 kcal mol^{-1} above the more stable isomer, at the B3LYP/BSI level, and will not be discussed in detail.

Note that, earlier, Sakaki et al.[30] studied the structure and stability of the η^1-C and η^2-coordinated isomers of $Ni(PH_3)_2(CO_2)$ at the Hartree−Fock, CI-SD, and MRCI-SD levels. These authors also found that, regardless of the level of calculation, the η^1-(C)-coordinated species is always less stable than the η^2-coordinated isomer.[30] The energy difference between these structures was found to be 23.3, 1.5, and 8.0 kcal mol^{-1} at the HF, limited CI-SD, and estimated full CI-SD levels, respectively. The result obtained in our paper, 8.5 kcal mol^{-1} (without ZPE), is in excellent agreement with 8.0 kcal mol^{-1}, at the estimated full CI-SD level by Sakaki and co-workers.[30]

As seen in Table 1, the calculated value of the CO_2- -$Ni(PH_3)_2$ bonding energy dramatically changes upon going from BSI to BSII: at B3LYP/BSI level it is almost 4.5 times overestimated compared to that at the B3LYP/BSII level. Furthermore, at the B3LYP/BSI level CO_2- -$Ni(PH_3)_2$ is about 7 kcal mol^{-1} stronger than the PH_3- -$Ni(PH_3)(CO_2)$, which incorrectly indicates that the active catalyst for the studied reactions should be the $Ni(PH_3)(CO_2)$ complex. However, by improving either the computational method (upon going from B3LYP/BSI to B3LYP/BSII) or the model [by going from $(CO_2)Ni(PH_3)_2$ to $(CO_2)Ni(PMe_3)_2$] the discrepancy between our results and common chemical sense is resolved. As seen in Table 1, (1) at the B3LYP/BSII level with ZPE the CO_2- -$Ni(PH_3)_2$ bonding energy, 4.6 kcal mol^{-1}, is about 3 times smaller than that for PH_3- -$Ni(PH_3)(CO_2)$, 13.1 kcal mol^{-1}. These data indicate that the active catalyst for the studied reactions 1−3 should be the $Ni(PR_3)_2$ complex. (2) Replacing R = H by R = Me increases the PR_3- -$Ni(PR_3)(CO_2)$ bonding energy from 13.1 (5.6) to 24.3 (12.3) kcal mol^{-1}. This trend is in excellent agreement with the experimental results of Nolan and co-workers,[31] who have shown that the increasing basicity of the P atom of the PR_3 ligand by varying R groups increases the metal−PR_3 bond strength. Therefore, (1) we expect that in the real system, $(CO_2)Ni(PCy_3)_2$, the weakest ligand attached to Ni is CO_2, and (2) since the B3LYP/BSI approximation may lead to wrong conclusions concerning energies, below we will focus only on the energetics calculated at the B3LYP/BSII level for discussion. Also, on the basis of the above presented points, in this and the next sections we will assume that the active catalyst is the linear $Ni(PR_3)_2$ species, modeled by $Ni(PH_3)_2$.

The structure and stability of $M(PR_3)_2$ complexes has been the subject of many studies[32] and, therefore, will not be discussed here in detail. Only one should note

(30) Sakaki, S.; Koga, N.; Morokuma, K. *Inorg. Chem.* **1990**, *29*, 3110.

(31) (a) Serron, S.; Nolan, S. P. *Organometallics* **1996**, *15*, 4301. (b) Serron, S.; Luo, L.; Stevens, E. D.; Nolan, S. P. *Organometallics* **1996**, *15*, 5209. (c) Li, C.; Luo, L.; Nolan, S. P. *Organometallics* **1996**, *15*, 3456. (d) Li, C.; Serron, S.; Nolan, S. P. *Organometallics* **1996**, *15*, 4020. (e) Li, C.; Ogasawara, M.; Nolan, S. P.; Caulton, K. G. *Organometallics* **1996**, *15*, 4900.

(32) (a) Obara, S.; Kitaura, K.; Morokuma, K. *J. Am. Chem. Soc.* **1984**, *106*, 7482. (b) Low, J. J.; Goddard, W. A., III. *J. Am. Chem. Soc.* **1986**, *108*, 6115. (c) Low, J. J.; Goddard, W. A., III. *Organometallics* **1986**, *5*, 609. (d) Hay, P. J. *Transition Metal Hydrides*; Dedieu, A., Ed.; VCH: Weinheim, 1992; pp 127−147, and references therein. (e) Musaev, D. G.; Morokuma, K. *Adv. Chem. Phys.* **1996**, V. XCV, pp 61−128.

that (1) in the complex $Ni(PR_3)_2$ the metal atom has the Ni(0) oxidation state with the (s^0d^{10}) configuration, which is about 36.3 kcal mol^{-1} higher than the ground state of the Ni atom, $^3D(s^1d^9)$. The stabilization of the d^{10} state takes place upon addition of two phosphines to the Ni atom, so that the ground state of $Ni(PR_3)_2$ becomes a linear d^{10} singlet. (2) The oxidative addition reaction A−B + $Ni(PR_3)_2$ → (A)(B)$Ni(PR_3)_2$ involves a change in the effective electronic configuration of Ni from a d^{10} configuration for $Ni(PR_3)_2$ to an s^1d^9 configuration for (A)(B)$Ni(PR_3)_2$; in other words, the metal atom is not oxidized during the addition of the A−B σ-bond, but rather the metal is promoted from the d^{10} state to the s^1d^9 state. (3) On the other hand, during the reductive elimination reaction (A)(B)$M(PR_3)_2$ → A−B + $M(PR_3)_2$ the electronic configuration of the M atom changes from s^1d^9 in (A)(B)$Ni(PR_3)_2$ to d^{10} in $Ni(PR_3)_2$. (4) The highest occupied orbital (HOMO) of $Ni(PR_3)_2$ is mainly the s+d_{z^2} orbital (*z*: P−Ni−P axis) of the metal atom. The low-lying unoccupied molecular orbitals (LUMOs) are Ni s−d_{z^2} and p orbitals. Upon P−Ni−P bending, the ordering of d orbital energies changes from that in the linear structure; most significantly, the d_{yz} (b_2) orbital (*z*: bisector of the P−Ni−P plane; *y*: in the P−Ni−P plane) becomes the HOMO. The HOMO along with the LUMO (a_1, roughly s−$d_{x^2-y^2}$) will interact with the vacant $\sigma(b_2)$ and $\sigma(a_1)$ orbitals of the A−B group, leading to the oxidative addition of A−B to the metal. Bearing the above discussions in mind, we can start our discussion on the mechanism of reactions 1−3.

B. Ammonium versus Iminium. We begin this section by analyzing two different mechanisms for the addition of allylammonium substrates to the Ni(0) catalyst, $Ni(PH_3)_2$. Later, we will make an analogous analysis for allyliminium substrates and compare the results for these two substrates.

Allylammonium Substrates. In general, the reaction may proceed via two distinct pathways (Scheme 2): dissociative and associative. The first of them starts with dissociation of one of the PH_3 ligands, followed by substrate coordination to the transition metal center, while the second proceeds without dissociation of PH_3 ligand prior to substrate coordination. Since PH_3 dissociation from $Ni(PH_3)_2$ is an energetically unfavorable process and requires about 35.1 kcal mol^{-1}, we will start our discussion with the associative pathway.

As seen in Scheme 2, after substrate coordination the associative path may split into two new paths, labeled path **A** and **B**. Both of them start from the same intermediate, $(CH_2{=}CHCH_2NH_3)Ni(PH_3)_2^+$, **1a**. The first step of path **A**, however, is dissociation of one of the phosphine ligands, followed by oxidative addition of the C−N bond to the Ni(0), while the first step of path **B** is oxidative addition of the C−N bond to the metal center. Hereafter, path **A** will be also referred to as the *dissociative* path, and path **B** as the *associative* path.

The prereactant complex **1a** is a metallacycle (Figure 3), where the Ni−C distances are 1.961 and 2.019 Å and the C=C and Ni−P bonds are 0.09 and 0.12 Å longer than those in the free $(CH_2{=}CHCH_2NH_3)^+$ and $Ni(PH_3)_2$ species, respectively (see Figure S-1 in the Supporting Information for geometries). The P−Ni−P angle is found to be 78° smaller than that in $Ni(PH_3)_2$. The dihedral angle between the P−Ni−P and C−Ni−C planes is 170°.

Scheme 2

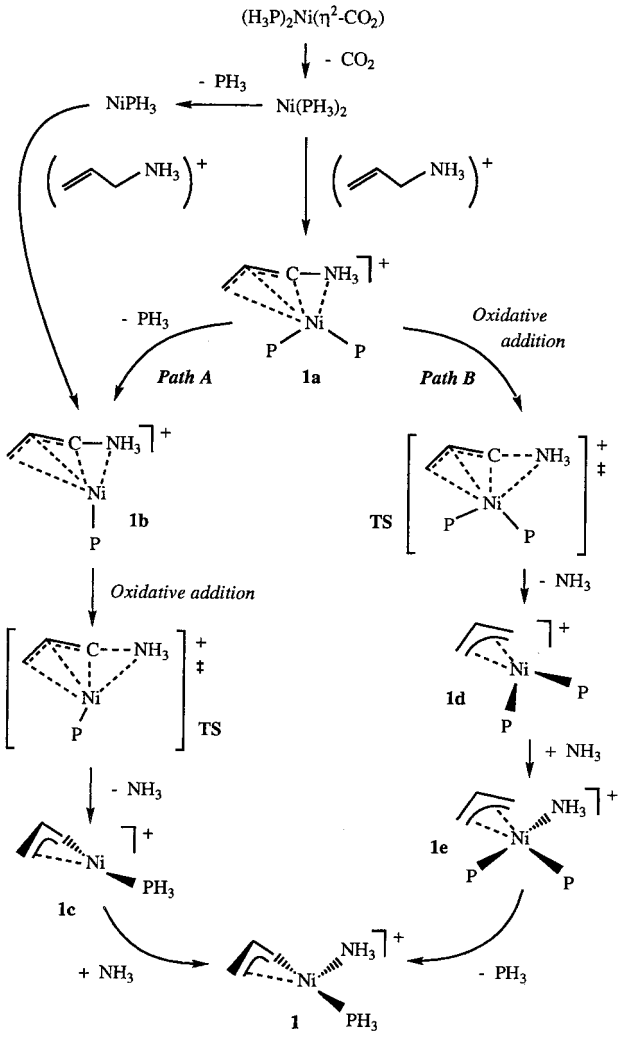

These large changes in the geometry suggest a strong interaction, which is borne out in the large calculated $(CH_2{=}CHCH_2NH_3)^+ + Ni(PH_3)_2$ complexation energy of −37.9 (−25.5) kcal mol^{-1}. All our attempts to locate other structures of complex $(CH_2{=}CHCH_2NH_3)Ni(PH_3)_2^+$ led to structure **1a**, where the metal strongly interacts with the C=C double bond to form a metallacycle.

As mentioned above, from **1a**, the reaction may proceed via two paths, dissociative and associative. The dissociation of one of the PH_3 ligands (path **A**) leads to the unsaturated three-coordinate complex **1b**. Attempts to locate a TS between **1a** and **1b**, namely **TS(1a→1b)**, have systematically led to either the reactant, **1a**, or the product, **1b**, which indicates the existence of no or a very small barrier (not studied further here). The other geometrical parameters change only slightly and will not be discussed. The **1a** → **1b** + PH_3 dissociation energy is calculated to be endothermic by 22.0 (11.5) kcal mol^{-1}, as shown in Table 2.

The next step on path **A** is the activation of the C−N bond. It takes place through the transition state **TS-(1b→1c)** given in Figure 3, where the C−NH_3, Ni−CNH_3, and NH_3C−C bonds (2.256, 2.898, and 1.412 Å, respectively) are 0.69 Å longer and 0.13 and 0.10 Å shorter than those in complex **1b** (see Figure S-1 for structural details). Normal-mode analysis confirms that

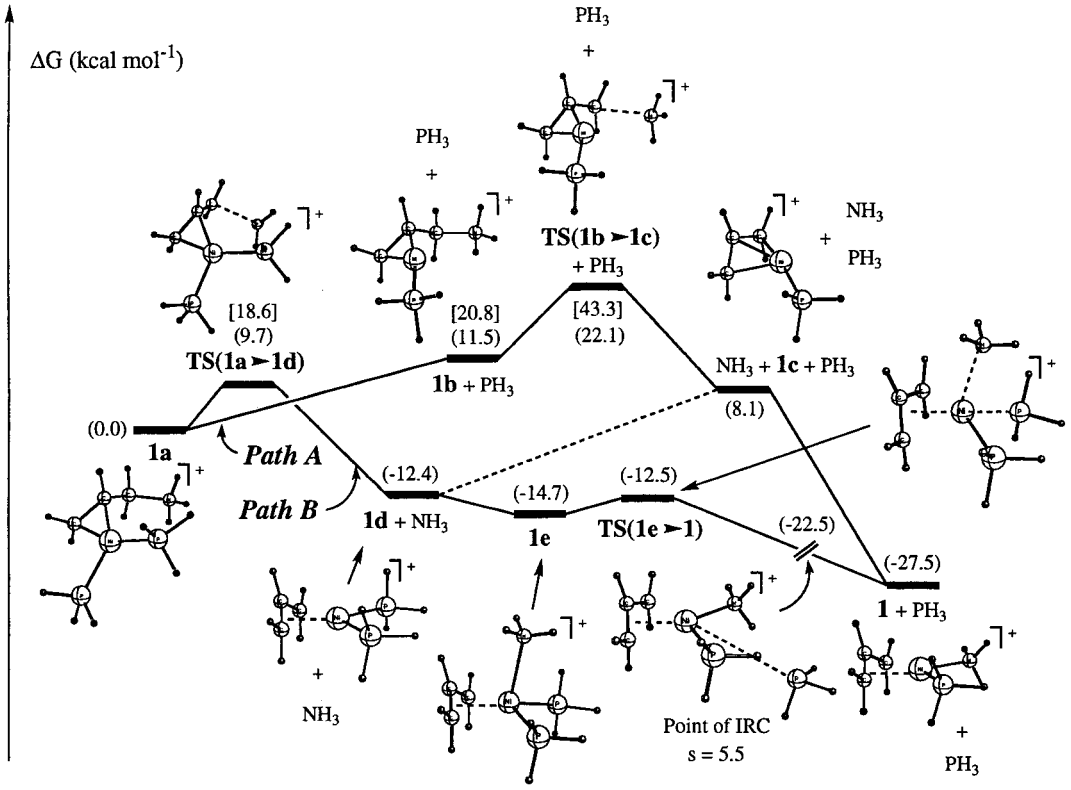

Figure 3. Potential energy profiles of the entire catalytic process for paths **A** and **B** of reaction 1. Gibbs free energies at 1 atm, 298.15 K (without solvent effects) relative to metallacycle **1a** are in parentheses. Free energies in solution (only for selected stationary points) are denoted in square brackets. All energies are in kcal mol^{-1}.

this is a real TS with one imaginary frequency, 208i cm^{-1}. It is interesting to note that the Ni−N distance increases from 3.254 to 3.361 Å as the reaction goes from molecular complex **1b** to **TS(1b→1c)**. This indicates that **TS(1b→1c)** does not lead directly to oxidative addition product **1** (where Ni−N = 1.986 Å) but to a precursor, **1c**, which arises from the NH_3 dissociation. This conclusion is supported by IRC calculations, which confirm that **TS(1b→1c)** connects molecular complexes **1b** and **1c** + NH_3. This reaction step is roughly thermoneutral, 6.0 (−3.4) kcal mol^{-1}. The barrier is calculated to be 10.8 (10.6) and 4.8 (14.0) kcal mol^{-1} relative to **1b** + PH_3 and **1c** + NH_3 + PH_3, respectively. All attempts to locate an oxidative addition TS have led to **TS(1b→1c)**. Therefore, it can be concluded that the lowest energy path connecting intermediate **1b** and product **1** proceeds through **TS(1b→1c)** and complex **1c**. In other words, recoordination of NH_3 to **1c** without barrier is found to be the final step on path **A**. Reaction 1 is calculated to be exothermic by 48.5 (48.6) kcal mol^{-1}.

The optimized structure of product **1**, in Figure 3, shows that NH_3, PH_3, and the allyl ligand are arranged in a square-planar fashion around the d^8 Ni center. The C−C bond *trans* to NH_3 (1.421 Å) is slightly longer than the C−C bond *trans* to PH_3 (1.416 Å), as expected from the relative σ-donor abilities of NH_3 and PH_3. Our results are also in good agreement with the experimental study by Aresta et al.,[12] where complex **1** has been characterized by IR spectroscopy and NMR techniques. The IR spectrum of **1** shows an absorption at 513 cm^{-1}, which strongly supports the presence of an allyl group π-coordinated to Ni. In addition, the $^{13}C\{^1H\}$ NMR spectrum of **1** is reported to present two different signals for the end carbon atoms of the allyl group. The latter result strongly indicates that these nuclei are not equivalent, discarding the possibility of a tetrahedral coordination to the metal atom.[12]

Aside from the path explored above, we have also investigated path **B**, as shown in Scheme 2, the first step of which is the activation of the C−N bond via the transition state **TS(1a→1d)**, leading to complex **1d**. The step is exothermic by 2.4 (12.4) kcal mol^{-1}. During this process, the C−N bond, being broken, is elongated from 1.565 Å in **1a** to 2.265 Å in the TS. In the meantime, the H_3NC−Ni bond, being formed, is shortened from 3.040 Å in **1a** to 3.021 Å in **TS(1a→1d)** and to 2.086 Å in **1d**. The Ni−NH_3 bond distance does not change significantly upon going from **1a** to **TS(1a→1d)**. Normal-mode analysis performed at the B3LYP/BSI level confirms that **TS(1a→1d)** is a real saddle point, with one imaginary frequency of 184i cm^{-1}. According to the IRC calculations, this TS connects structures **1a** and **1d** + NH_3. This means that **TS(1a→1d)**, similarly to **TS(1b→1c)** in the case of path **A** discussed above, is the TS for NH_3 elimination rather than the TS for oxidative addition of the CH_2CHCH_2- -NH_3 bond. The activation barrier is calculated to be 10.5 (9.7) kcal mol^{-1} relative to **1a** and 12.9 (22.1) kcal mol^{-1} relative to **1d** + NH_3.

Formation of product **1** from **1d** may take place through two different paths: (i) either by direct PH_3 dissociation followed by NH_3 coordination (dashed line in Figure 3) or (ii) by a NH_3 coordination to give the pentacoordinated complex $(PH_3)_2Ni(NH_3)(C_3H_5)^+$, **1e**, followed by dissociation of one of the PH_3 groups. The former process, **1d** + NH_3 → **1c** + NH_3 + PH_3 → **1** + PH_3, is energetically unfavorable (requiring about 30.4

(20.5) kcal mol^{-1} for phosphine dissociation) and will be excluded from further discussions. On the other hand, our calculations reveal that the **1d** → **1** process can take place via the second path, i.e., **1d** + NH_3 → **1e** → TS → **1** + PH_3; the coordination of the NH_3 ligand to complex **1d** is exothermic by 11.8 (2.3) kcal mol^{-1} and leads to the stable pentacoordinated complex **1e**, where the apical position of the square pyramid around Ni is occupied by the NH_3 ligand with a Ni−NH_3 distance of 2.378 Å (Figures 3 and S-1). Note that upon coordination of NH_3 to **1d**, the geometry of the latter does not change significantly. The resulting complex **1e** has C_s symmetry with two equal Ni−P and C_c−C_t bonds (where C_c and C_t stand for the central and terminal carbon atoms of the allyl fragment, respectively). Such a pentacoordinated structure is not unknown in the chemistry of the Ni triad. The existence of pentacoordinated intermediates of low-valent Ni and Pd complexes has been reported earlier.[33]

Complex **1e** is 4.6 (12.8) kcal mol^{-1} higher than product **1** + PH_3 and is separated from the latter by a 1.4 (2.2) kcal mol^{-1} barrier at the TS **TS(1e→1)**, corresponding to PH_3 dissociation. Figure 3 shows a structure taken from the IRC path (s = 5.5 amu$^{1/2}$ bohr) to illustrate the concerted NH_3-rearrangement−PH_3-release; this structure is ca. 22.5 kcal mol^{-1} below **1a**. Dissociation of PH_3 in **1e** is favored over dissociation of NH_3. Support for this statement comes from the corresponding binding energies in product **1**, where it is also found that removal of PH_3 costs less than removal of NH_3 (BE_{Ni-P} = 33.1 kcal mol^{-1}, BE_{Ni-N} = 49.0 kcal mol^{-1}).

The overall free energy profiles of the entire catalytic process for paths **A** and **B** are also shown in Figure 3. As seen from this figure, the rate-determining step of path **A** is the PH_3 dissociation from **1a**, which requires 22.0 (11.5) kcal mol^{-1}, closely followed by **TS(1b→1c)**, while the rate-determining step of path **B**, C−N activation of allylammonium substrates, is energetically less demanding, requiring only 10.5 (9.7) kcal mol^{-1}, than PH_3 dissociation. Therefore, by comparing the bottleneck in path **B** (10.5 (9.7) kcal mol^{-1}) with the endothermicity of the PH_3 dissociation from complex **1a** (22.0 (11.5) kcal mol^{-1}) in path **A**, it can be deduced that PH_3 dissociation will preferably take place *after* C−N activation, and consequently, the *associative* mechanism depicted in path **B** is more likely to operate than the dissociative mechanism in path **A**.

Does the consideration of solvent affect the validity of this conclusion? Is path **B** still more likely to operate than path **A** in the presence of solvent? Since real experiments are not conducted in a vacuum but in THF,[12] a more accurate description for this reaction should be obtained by adding a polarized continuum model[27] with the dielectric constant of THF (ϵ = 7.58) to our gas-phase models. Single-point calculations on the optimized structures of intermediates **1a** and **1b** and TSs **TS(1a→1d)** and **TS(1b→1c)** embedded in a cavity simulating the interactions with THF yielded the free energies in solution shown in square brackets in Figure 3. As can be seen, the energy profiles for paths **A** and **B** are scaled upon addition of solvent, but the relative energy differences remain unchanged. It follows that solvent effects do not change the previous conclusion; path **B** is the operative one also in solution.

Scheme 3

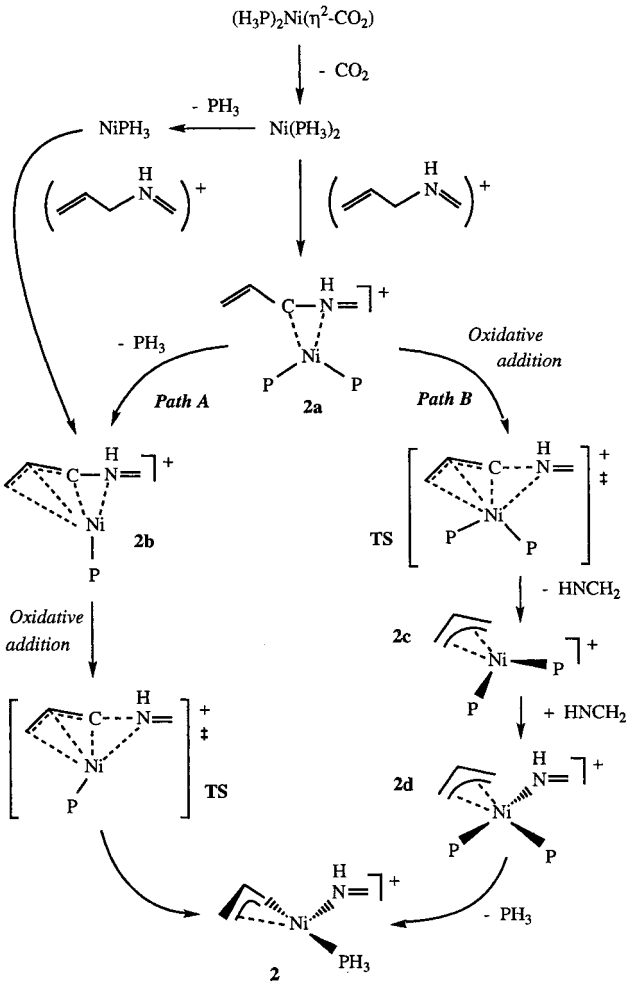

One should note that, although our theoretical studies suggest that NH_3 dissociates through transition state **TS(1a→1d)** during the reaction **1a** → **1** + PH_3, no spectroscopic evidence was found for the formation of carbamic acid derivatives when reaction I.b (see Scheme 1) was carried out under a CO_2 atmosphere,[12] which suggests that the lifetime of **1d** is very short, if it exists. Since, as shown in Figure 3, recoordination of NH_3 to **1d** to form **1e** is an exothermic process by 2.3 kcal mol^{-1} and takes place without barrier, we may expect that dissociation and recombination of NH_3 occur very fast, which excludes the existence of free NH_3 during the reaction and makes our results consistent with the available experiment.

Allyliminium Substrates. Let us now discuss the oxidative addition of allyliminium to $Ni(PR_3)_2$, reaction 2. For this reaction we follow mechanisms (Scheme 3) analogous with those discussed above for reaction 1.

As in the case of the allylammonium cation, the first step of reaction 2 is likely to be complexation of the organic substrate, $(CH_2{=}CHCH_2HN{=}CH_2)^+$, to $Ni(PH_3)_2$ to give a metallacycle. However, unlike in reaction 1, here we found such a metallacycle in two different isomeric forms, **2a** and **2a′**, corresponding to the coordination of the allyliminium cation to the Ni center via its N=C and C=C double bonds, respectively

(33) Fan, L.; Krzywicki, A.; Somogyvari, A.; Ziegler, T. *Inorg. Chem.* **1996**, *35*, 4003, and references therein.

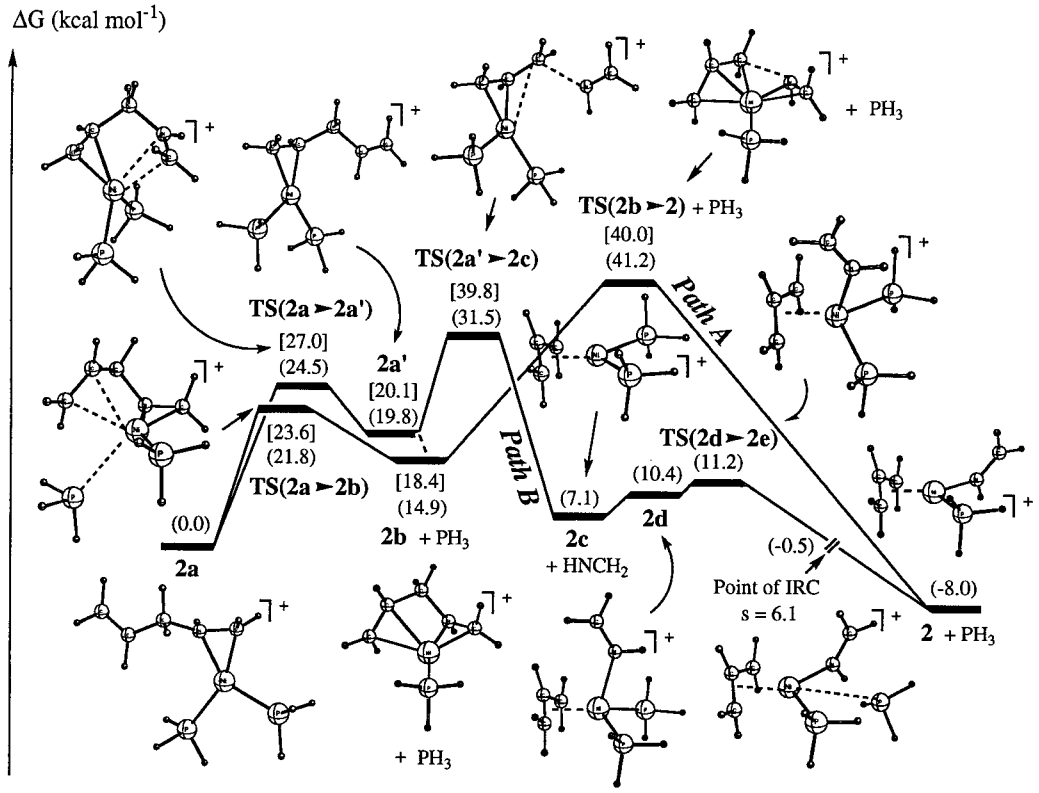

Figure 4. Potential energy profiles of the entire catalytic process for paths **A** and **B** of reaction 2. Gibbs free energies at 1 atm, 298.15 K (without solvent effects) relative to metallacycle **2a** are in parentheses. Free energies in solution (only for selected stationary points) are denoted in square brackets. All energies are in kcal mol^{-1}.

(see Figure 4). The more stable is found to be **2a**, which lies 19.2 (19.8) kcal mol^{-1} below isomer **2a′** (Table 3). This difference in stability can be ascribed to the stronger Ni−N than Ni−C interaction because of stronger donating capability of N. As seen in Figure S-2 (structural details are given in the Supporting Information), Ni−C_t and Ni−C(H) bonds in **2a′** are 0.05 and 0.07 Å longer than Ni−C_t and Ni−N in **2a**, respectively. Also, the N═C bond is stretched to a larger extend than the C═C bond in **2a′** relative to the free allyliminium cation (0.142 versus 0.088 Å, in **2a** and **2a′**, respectively). The conversion from **2a** to **2a′** requires a barrier of 23.9 (24.5) kcal mol^{-1} at **TS(2a→2a′)**. Normal-mode analysis confirms that **TS(2a→2a′)** is a real saddle point, with an imaginary frequency of 97i cm^{-1}. The $(CH_2{=}CHCH_2{-}HN{=}CH_2)^+ + Ni(PH_3)_2$ complexation energy for the more stable isomer **2a** is calculated to be 54.4 (43.5) kcal mol^{-1}.

As shown in Figure 4, starting with the most stable isomer, **2a**, the reaction may split again into two different paths: dissociative (**A**) and associative (**B**). The first step of path **A** is the dissociation of one of the PH_3 ligands leading to complex **2b** via **TS(2a→2b)**. One might expect that **2b** (Figure 4) adopts a structure similar to **1b** (Figure 3), but **2b** is found to be an unsaturated three-coordinate complex; the terminal C═C double bond of the organic chain rotates and occupies the empty site of the metal. The PH_3 dissociation from **2a** to give **2b** is endothermic by 24.1 (14.9) kcal mol^{-1} (Table 3) and has an activation barrier of 26.5 (21.8) kcal mol^{-1}.

The next reaction step is the C−N bond activation, which takes place through transition state **TS(2b→2)** in Figure 4. At the TS, the C−N(H)C_tH_2 and Ni−N bonds (2.032 and 2.132 Å, respectively) are 0.525 and 0.198 Å longer than those in complex **2b**. Also, the terminal C═C bond in **2b** (1.367 Å) is elongated by 0.04 Å at **TS(2b→2)** (1.405 Å), while the Ni−C_c and Ni−C_t bonds (2.370 and 2.445 Å, respectively, in **2b**) are strengthened at the TS (2.050 Å Ni−C_c and 2.131 Å Ni−C_t). Normal-mode analysis confirms that this structure has one imaginary frequency, 374i cm^{-1}, and IRC calculations indicate that **TS(2b→2)** connects **2b** with product **2**. The barrier height at **TS(2b→2)** measured from **2b** is 24.2 (26.3) kcal mol^{-1}.

The optimized geometry of product **2** shown in Figures 4 and S-2 (Supporting Information) indicates that only the N atom of the $(NHCH_2)^+$ ligand is linked to the metal center (Ni−N = 1.926 Å, Ni−C = 2.934 Å, ∠Ni−N═C = 130.2°), even though it is known that coordination of imines to metal centers may involve either the nitrogen atom (η^1(N))[34] or both the N and C atoms (η^2-(C,N)).[35] Our optimized geometry is in good agreement with the experimentally[12] reported ^{13}C NMR spectrum of **2**, which unambiguously establishes that the imine ligand mode of bonding is η^1(N).

Next we discuss path **B**. The first "natural" step in path **B** should be the activation of the C−N bond directly on **2a**. However, cleavage of the C−N bond at **2a** is found to be kinetically prohibitive, with an activation barrier of 38.8 (39.4) kcal mol^{-1} (see "TS_{C-N} from **2a**" in Figure S-2, and also in Table 3). We have

(34) (a) Cini, R.; Caputo, P. A.; Intini, F. P.; Natile, G. *Inorg. Chem.* **1995**, *34*, 1130. (b) Fogg, D. E.; James, B. R. *Inorg. Chem.* **1995**, *34*, 2557.

(35) (a) Buchwald, S. L.; Watson, B. T.; Wannamaker, M. W.; Dewan, J. C. *J. Am. Chem. Soc.* **1989**, *111*, 4486. (b) Meyer, J. M.; Curtis, C. J.; Bercaw, J. E. *J. Am. Chem. Soc.* **1983**, *105*, 2651.

not explored further this route involving such a demanding TS. As depicted in Figure 4, an alternative way to initiate path **B** from **2a** consists of proposing, first, isomerization from **2a** to **2a′** and, then, activation of the C−N bond at **2a′**. Isomerization from **2a** to **2a′** has already been discussed above; the energy required to overcome the barrier at **TS(2a→2a′)** is not small, 23.9 (24.5) kcal mol^{-1}, but at least it is less than the barrier of 38.8 (39.4) kcal mol^{-1} at "TS_{C-N} from **2a**". Once **2a′** is formed, C−N activation could take place via the transition state **TS(2a′→2c)**, which is 14.8 (11.7) kcal mol^{-1} above **2a′**, and leads to bisphosphine complex **2c** + $HNCH_2$. Recoordination of the $HNCH_2$ fragment to **2c** to yield a pentacoordinated allyl−Ni−imine complex **2d** is nearly thermoneutral (in terms of enthalpy, exothermic by 8.4 kcal mol^{-1}; in terms of free energy, endothermic by 3.3 kcal mol^{-1}). The corresponding barrier (not reported here) is expected to be small. In complex **2d** the ligands adopt a square-pyramidal arrangement around the Ni center, with the apical site occupied by the $NH{=}CH_2$ ligand.

Final formation of product **2** from **2d** requires dissociation of PH_3 *and* shift of the NH_3 ligand from the apical position to the equatorial plane. Both processes occur concertedly through an early TS, **TS(2d→2)**, which lies only 0.7 (0.8) kcal mol^{-1} above **2d**. IRC calculations on the product side reveal that **TS(2d→2)** undergoes imine rearrangement and releases one PH_3 ligand to yield product **2** without any additional intermediate in between. (Figure 4 shows a structure on the IRC path to illustrate the concerted imine rearrangement−PH_3 release; this point corresponds to the length of IRC $s = 6.1$ amu$^{1/2}$ bohr and lies 0.5 kcal mol^{-1} below **2a.**)

The free energy profile of the entire catalytic process (eq 2) (paths **A** and **B**) is shown in Figure 4. For the sake of clarity, direct activation of the C−N bond at **2a** (via "TS_{C-N} from **2a**") has not been depicted in this figure. As already mentioned, such a step is computed to be kinetically prohibitive, with a high barrier of 38.8 (39.4) kcal mol^{-1}, and therefore is very unlikely to be part of the operative mechanism.

Putting all these together, only two mechanisms are feasible candidates for this reaction (path **A** and path **B** as depicted in Figure 4). Considered as a whole, path **B** seems less energy demanding than path **A**. This notwithstanding, observed in detail there are two drawbacks that make path **B** unfavorable. (1) The activation energy for the isomerization step **2a** → **2a′**, 23.9 (24.5) kcal mol^{-1}, is on the borderline for a catalytic reaction, and (2) the small barrier for the reverse reaction (**2a′** → **2a**), 4.7 (4.7) kcal mol^{-1}, tends to keep the equilibrium back toward formation of **2a** instead of promoting the reaction to move forward. In this sense, the situation for the first step of path **A** looks better; the barrier is slightly lower, 26.5 (21.8), and **2b** is stable enough not to turn back into **2a**. The bottleneck in path **A**, however, is encountered in the second step; with the current models the barrier height at **TS(2b→2)** measured from **2b** is still 24.2 (26.3) kcal mol^{-1}.

To see whether the presence of bulkier ligands (as in the real system) would reduce this barrier, either by stabilizing **TS(2b→2)** or by destabilizing intermediate **2b**, we have performed a separate ONIOM study for species **2b** and **TS(2b→2)**. In this study we have used the real, experimentally reported, system. Two types of ONIOM combination have been selected: (a) an MO + MM (universal force field, UFF)[36] combination denoted below as O1, ONIOM(B3LYP/BSI:UFF), to assess *only* the steric effects from the bulky PCy and Me groups, and (b) an MO + MO combination denoted below as O2, ONIOM(B3LYP/BSI:HF/LANL2MB), to evaluate *both* steric *and* electronic effects. In both ONIOM calculations, the model complex used throughout the section was treated both at the higher and at the lower level of the combination, and the real system was treated only at the lower level. The results are shown in Figure 5.

Our calculations reveal that inclusion of neither steric effects nor electronic effects reduces the barrier height. The barriers calculated at the O1 and O2 levels of theory are 27.2 and 32.9 kcal mol^{-1}, respectively, versus 29.7 kcal mol^{-1} (BSI without ZPE) for the model system. The origin of this finding can be traced by inspection of Figure 5. The addition of bulkier ligands in **2b** weakens the π-bonding interaction between Ni and C=C (which is much stronger in the small model of **2b**, Figures 4 and S-2, 2.4 Å, than in **2b/O1** and **2b/O2** intermediates, 3.2−3.8 Å) and therefore destabilizes the complex (see Figure 5). This notwithstanding, the TS is destabilized as much as (or stronger than) **2b** due to the addition of bulkier ligands. To better accommodate the allyl fragment closer to the metal center as the reaction proceeds from **2b** to TS, one of the cyclohexyl rings in the phosphine is forced to rotate (see Figure S-4 in the Supporting Information for detail). Such a rotation shortens the distance between the three Cy's of the phosphine, which are in the same plane in the TS, and increases the repulsion between them. In **2b**, the allyl fragment is far enough away from the metal center to allow the corresponding Cy ring to remain perpendicular so that the contact with its neighbors is minimum. The net effect is that the activation energy is comparable or larger with substituents than without. The addition of bulkier ligands does not reduce the rate-determining step of reaction 2.

The next question we examined is the role of solvent. Since experiments were conducted in THF,[12] we have performed single-point calculations on the optimized structures of intermediate **2b** and **TS(2b→2)** embedded in a cavity simulating the interactions with THF (dielectric constant = 7.58) using a polarized continuum model.[27] In Figure 4, free energies including solvent effects (i.e., in solution) are given in square brackets. The calculated free-energy barrier for **2b** → **TS(2b→2)** is reduced from 26.4 kcal mol^{-1} in the gas phase to 21.6 kcal mol^{-1} in solution. This indicates that under real conditions the step **2b** → **2** is less energy demanding than initially computed and, therefore, is more probable. Moreover, similar single-point calculations including solvent effects on **TS(2a→2a′)**, **2a′**, and **TS(2a′→2c)** resulted in an increase of the barriers for the first two steps of path **B**, from 24.5 to 27.0 kcal mol^{-1} for the first step, and from 11.7 to 19.7 kcal mol^{-1} for the second step. Thus, inclusion of solvation effects makes path **A** more favorable than path **B** for reaction 2.

(36) Rappé, A. K.; Casewit, C. J.; Colwell, K. S.; Goddard, W. A., III; Skiff, W. M. *J. Am. Chem. Soc.* **1992**, *114*, 10024.

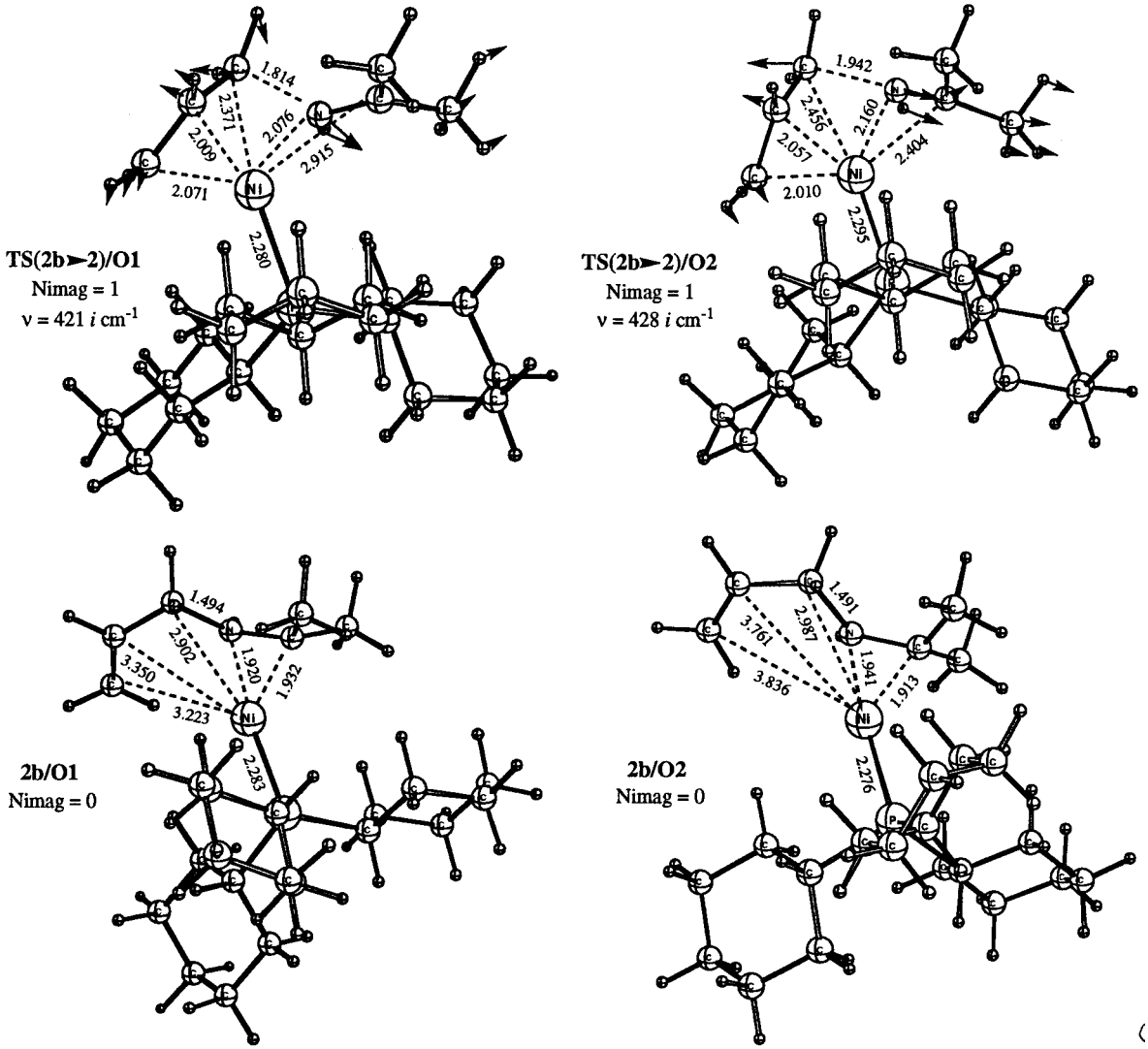

Figure 5. Fully optimized geometries (Å and deg) of intermediate **2b** and transition state **TS(2b→2)** with real substituents ($-PCy_3$ and $-N{=}CMe_2$) at two different levels: (a) ONIOM(B3LYP/BSI:UFF), denoted as O1; and (b) ONIOM(B3LYP/BSI:HF/LANL2MB), denoted as O2.

Comparison of Ammonium (1) and Iminium (2) Reactions. The above-presented results show that the reactions of $Ni(PH_3)_2$ with allylammonium and allyliminium cations follow different mechanistic patterns. The reaction of allylammonium substrates with the catalyst takes place through NH_3 dissociation (or oxidative addition of the C−N bond to the bisphosphine catalyst) as the first reaction step (associative mechanism), whereas the corresponding reaction of allyliminium substrates proceeds via phosphine dissociation as the first step (dissociative mechanism).

To understand the sources of this difference, we should keep in mind two factors: (1) the BE's of the C−N bonds to be cleaved, which are related to the chemical nature of these bonds, and (2) the BE's for PH_3, i.e., the energies for phosphine dissociation. In the case of allylammonium substrates, $CH_2CH(H_2)C-NH_3^+$, the linkage between the C and N atoms is based on a donor−acceptor interaction. Breaking the C−N bond at the allylammonium substrate involves less energy, 10.5 (9.7) kcal mol^{-1}, than removing a PH_3 ligand from the metal center of the catalyst, 22.0 (11.5) kcal mol^{-1}. Given the small difference, both paths, associative and dissociative, could be regarded as feasible, but the *most likely* mechanism of the reaction of $Ni(PH_3)_2$ with allylammonium is the associative mechanism, path **B**, which involves (1) coordination of substrate to the transition metal center to give **1a**, (2) elimination of NH_3 with formation of allyl−$Ni(PH_3)_2^+$, **1d**, (3) quick recoordination of NH_3 to the transition-metal center to give a pentacoordinated species, **1e**, and (4) dissociation of one of the phosphine ligands to give product **1**.

On the contrary, the interaction between the allyl and the iminium group in the allyliminium cation is a typical covalent bond. The larger strength of this bond (BE_{C-N} = 86.1 kcal mol^{-1} calculated at B3LYP/BSI level without ZPE) as compared to the allyl−NH_3 bond in the allylammonium cation (BE_{C-N} = 57.7 kcal mol^{-1}, same level, also without ZPE) causes a higher activation barrier for the reaction involving C−N bond cleavage (oxidative addition) at allyliminium cation **2a**, 38.8 (39.4) kcal mol^{-1} for TS_{C-N} from **2a**, not shown in Figure 4. Despite that, this is an oxidative addition process leading to a very stable pentacoordinated intermediate, **2d**, which requires a very high activation barrier, even higher than phosphine dissociation energy; the phosphine dissocia-

tion at **2a** requires only 24.1 (14.9) kcal mol^{-1}. Therefore, the reaction with allyliminium cation **2a** most likely will proceed in a dissociative fashion (path **A**) rather than associative (path **B**). The operative mechanism of this reaction includes (1) coordination of allyliminium to the Ni center of $Ni(PH_3)_2$ to give **2a**, (2) dissociation of one of the phosphine groups, and (3) oxidative addition of the allyliminium bond to give the final product, **2**. The rate-determining step of this reaction is found to be C−N activation for both the model phosphine ligand PH_3 and for the real phosphine group PCy_3. However, it may change for bidentate phosphines, where the dissociation of one of the phosphine "legs" could be an energetically demanding process. Therefore, we can expect a markedly different effect from the excess of phosphine on the reactions with allylammonium and allyliminium complexes. In the former case, the rate of the reaction will not be much altered, whereas, in the latter case, addition of phosphine may dramatically reduce the catalytic efficiency of the process to the point of completely inhibiting the reaction. Also, changing the polarity of the solvent may modify the course of the reaction.

One should note that the above-presented data suggest that reaction 1 will take place under mild conditions, whereas reaction 2 is an energy-demanding process and needs special conditions to take place. Our conclusions on reaction 2 are not consistent with available experiment (the *mechanistic* conclusions, however, are valid). At the present levels of calculation, even with the inclusion of solvent, there is no clear explanation for this discrepancy between theory and experiment. Further work is in progress.

C. C−N Activation versus N−H Activation. Up to this point, we have discussed C−N bond activation in the allylammonium and allyliminium cations by a Ni(0) complex, which is the only experimentally observed process (see Scheme 1). No processes corresponding to the N−H bond activation have been reported for the present allyl systems. The absence of products derived from N−H cleavage in the case of allylammonium substrates can be directly related to the hydrogen atom donor ability of amines. It is well-known[2c,37] that the N−H bond enthalpy in ammonia and primary amines is 107 and 88−100 kcal mol^{-1}, respectively. These data already suggest that ammonia and amines are very poor as hydrogen atom donors. Note that relatively few examples of N−H activation of ammonia by a metal center in solution have been reported.[38,39] Herein, N−H bond activation will be discussed only for allyliminium substrates (reactions 3-c and 3-t).

Table 4 shows the energetics of reaction 2 (path **B**), corresponding to C−N bond activation, and for the pair of reactions 3-c and 3-t, corresponding to the unobserved N−H bond activation. As seen in Table 4, all three processes are exothermic; reaction 2 is computed to be only slightly more favorable than reactions 3-c and 3-t. Therefore, the reason C−N bond activation is preferred over N−H must be found in the kinetics of these reactions.

The sequence of intermediates (and TSs) calculated for reactions 3-c and 3-t is depicted in Figure 6. The first reaction step to take place can be considered the same as for reaction 2, i.e., the coordination of the organic substrate $[(CH_2{=}CHCH_2)HN{=}CH_2)]^+$ to $Ni(PH_3)_2$ to give a metallacycle **3a** (= **2a**). This complex can be regarded as the branch point from where either C−N cleavage (Figure 3) or N−H cleavage occurs. Figure S-3 (Supporting Information) shows the optimized structures of intermediates and TSs for the N−H cleavage process.

To place the two phosphine ligands in the hydrido-imino product *cis* to each other, structure **3-*cis***, the attack of $Ni(PH_3)_2$ on the N−H bond must take place in a coplanar fashion. Figure 6 shows the three-centered TS corresponding to this attack. Normal-mode analysis confirms that such a three-membered structure has one imaginary frequency, 245i cm^{-1}. As can be seen, the N−H bond in **TS(3a→3-*cis*)** has stretched to 1.146 Å (from 1.022 Å in **3a**), whereas the Ni atom has notably approached the H atom (from 2.539 Å in **3a** to 1.708 Å), without losing the interaction with the N atom. Also, the Ni−C distance has increased (to 2.885 Å from 1.916 Å in **3a**), and the C−N bond has slightly decreased (to 1.337 Å from 1.435 Å in **3a**). Such geometrical parameters clearly indicate that at **TS(3a→3-*cis*)** (i) the π-interaction between the metal center and the C=N double bond has weakened to the point of being almost nonexistent, whereas (ii) a weak η^2-NH coordination (here better described as a kind of agostic interaction) has been formed between the Ni center and the bond to be cleaved. The barrier height for the process **TS(3a→3-*cis*)** is calculated to be 44.7 (43.9) kcal mol^{-1}, as shown in Figure 6. This high barrier might result mainly from the loss of the π-interaction mentioned in point (i) which cannot be compensated by the poorly forming Ni···N and Ni···H interactions in point (ii). Thus, the formation of the product **3-*cis***, $[cis\text{-}(H)Ni(PH_3)_2(\eta^1(N)\text{-}CH_2{=}CHCH_2N{=}CH_2)]^+$, is kinetically prohibitive.

Known examples of N−H activation have been reported for ammonia, amines, and amides.[40] However, no similar reactions have been reported for imines, the only exception being, to the best of our knowledge, the recent example reported by Aresta et al.[12] where for the first time an iminium cation carrying an *aryl* group has been observed to undergo N−H activation. In that case, a *trans*-bis(phosphine)−hydrido−imino complex has been isolated and characterized. According to this, another possibility involving N−H activation (Figure 6) is precisely the formation of the hydrido−imino complex with the two phosphine ligands *trans* to each other, **3-*trans***. Direct formation of complex $[trans\text{-}(H)Ni(PH_3)_2\text{-}(\eta^1(N)\text{-}CH_2{=}CHCH_2N{=}CH_2)]^+$, however, would involve the $Ni(PH_3)_2$ catalyst and the iminium substrate inter-

(37) McMillen, D. F.; Golden, D. M. *Annu. Rev. Phys. Chem.* **1982**, *33*, 492.

(38) (a) Koelliker, R.; Milstein, D. *Angew. Chem., Int. Ed. Engl.* **1991**, *30*, 707. (b) Banaszak Holl, M. M.; Wolczanski, P. T.; Van Duyne, G. D. *J. Am. Chem. Soc.* **1990**, *112*, 7989. (c) Roesky, H. W.; Bai, Y.; Noltemeyer, M. *Angew. Chem.* **1989**, *101*, 788; *Angew. Chem., Int. Ed. Engl.* **1989**, *28*, 754. (d) Bercaw, J. E.; Davies, D. L.; Wolczanski, P. T. *Organometallics* **1986**, *5*, 443. (e) Hillhouse, G. L.; Bercaw, J. E. *J. Am. Chem. Soc.* **1984**, *106*, 5472. (f) S¸ss-Fink, G. Z. *Naturforsch., B: Chem. Sci.* **1980**, *35*, 454. (g) Armor, J. N. *Inorg. Chem.* **1978**, *17*, 203. (h) Bryan, E. G.; Johnson, B. F. G.; Lewis, J. *J. Chem. Soc., Dalton Trans.* **1977**, 1328.

(39) Casalnuovo, J. C.; Calabrese, J. C.; Milstein, D. *Inorg. Chem.* **1987**, *26*, 971.

(40) (a) Milstein, D.; Schulz, M. *J. Chem. Soc., Chem. Commun.* **1993**, 318. (b) Schaad, D. R.; Landis, C. R. *Organometallics* **1992**, *11*, 2024. (c) Gagné, M. R.; Stern, C. L.; Marks, T. J. *J. Am. Chem. Soc.* **1992**, *114*, 275.

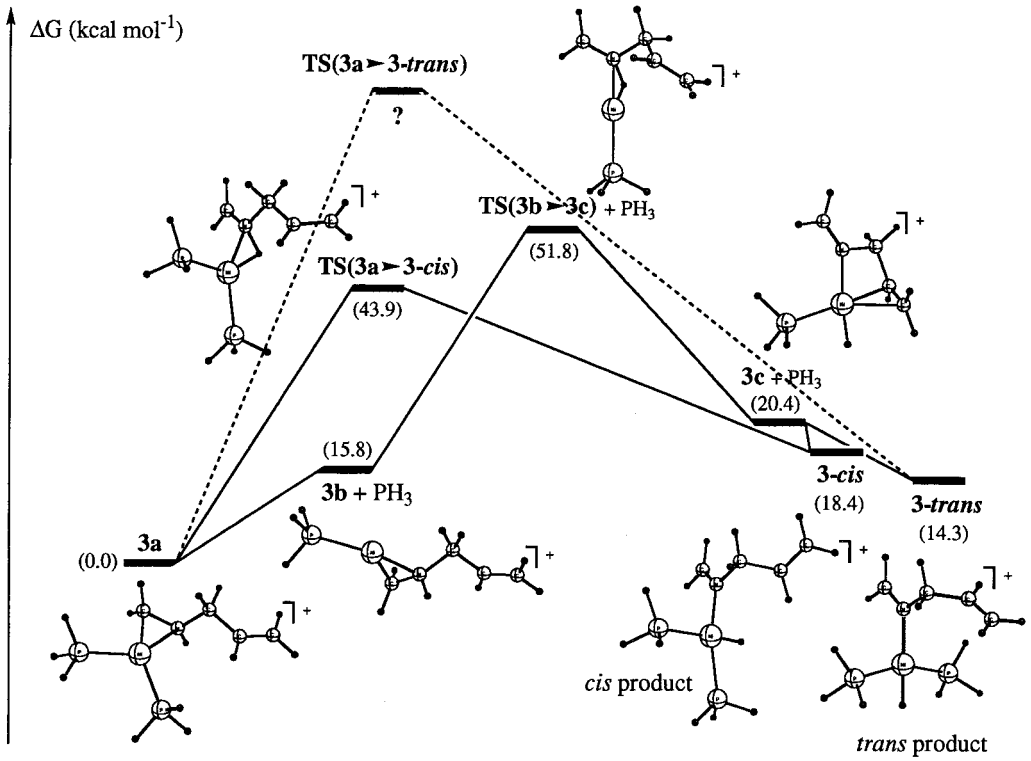

Figure 6. Potential energy profiles of the catalytic processes leading to products **3-*cis*** and **3-*trans***. Gibbs free energies relative to metallacycle **3a** (in parentheses) are in kcal mol^{-1}.

acting in perpendicular planes, which is expected to be even more energetically costly than the coplanar attack described above for the *cis* isomer. One way to avoid such a high-energy demanding process is by dissociation of one of the PH_3 groups leading to complex **3b** and activation of the N−H bond followed by recombination of the leaving PH_3 group. The first step of the reaction, PH_3 dissociation, is found to be endothermic by 25.4 (15.8) kcal mol^{-1} (Table 5).

Once complex **3b** is formed, cleavage of the N−H bond leads to the d^8 complex **3c** (Figure 6). Interestingly, species **3c** is not an unsaturated three-coordinate complex. The unsaturated complex has been also optimized and found to lie 18.9 kcal mol^{-1} above **3c**, having a distorted T-shape structure with ∠H−Ni−N = 172.0°, ∠H−Ni−P = 76.0°, ∠P−Ni−N = 112.0°, a short Ni−P bond (2.206 Å), and a terminal hydride (Ni−H = 1.468 Å) almost coplanar to the NNiP plane. Rotation of the allyl skeleton to occupy the vacant site at the metal center prevents **3c** from being a highly unstable intermediate. It should be noted that the terminal C=C double bond has approached the Ni center (on average, Ni−C = 2.184 Å) and that the Ni−P bond, which is *trans* to the C−C interaction, has slightly shortened (from 2.284 Å in **3b** to 2.265 Å). The Ni−H distance in **3c** (1.466 Å) is typical of a nickel hydride.

From **3c**, either **3-*cis*** or **3-*trans*** can, in principle, be formed, although the addition of PH_3 to yield the latter becomes more exothermic by 5.1 (6.1) kcal mol^{-1} (Table 4). A few nickel(II) complexes with a terminal hydride, also stabilized by two tricyclohexylphosphine ligands but without any iminium ligand, have been isolated and characterized.[41] In most cases the isolated species has been the *trans* isomer. In our case, **3-*trans*** can be obtained either directly from **3b** → **3c** or by isomerization of **3-*cis*** (via **3c**), both paths involving **3c**. Concerning the viability of the step **3b** → **3c**, only if the activation barrier associated with this process is low enough, will the chance to obtain **3c** be large, and N−H bond activation (through this path) will be able to compete with C−N oxidative addition.

The intermediacy of complex **3b** in the path from **3a** to product **3-*trans*** is expected to assist the kinetics of the reaction by preventing the N−H bond from being attacked perpendicularly. Such an attack would be very unfavorable from a molecular orbital point of view. To evaluate how facilitated the slipping of the coordinated iminium becomes after the loss of one PH_3 ligand, let us analyze **TS(3b→3c)** in Figure 6. At this point, an η^2(NH) coordination between the Ni center and the N−H bond has been formed, whereas the π-interaction of Ni with the C=N double bond has been much weakened. Compared with **TS(3a→3-*cis*)**, **TS(3b→3c)** is more product-like, as revealed by the longer N−H and the shorter Ni−H distance (1.276 and 1.605 Å, respectively). However, counterbalancing bond-forming and bond-breaking processes leads to a result not much different from the one obtained for product **3-*cis***. The energy barrier for **TS(3b→3c)** is computed to be 36.6 (36.0) kcal mol^{-1} (Figure 6). This means that the above-mentioned slipping is slightly easier when only one PH_3 ligand is attached to Ni, but is still very costly. Therefore, formation of products **3-*cis*** or **3-*trans*** through this route is also kinetically impeded.

In conclusion, whether the oxidative addition step is formulated to occur with a monophosphine− or a

(41) (a) Darensbourg, M. Y.; Ludwig, M.; Riordan, C. G. *Inorg. Chem.* **1989**, *28*, 1630. (b) Imoto, H.; Moriyama, H.; Saito, T.; Sasaki, Y. *J. Organomet. Chem.* **1976**, *120*, 453. (c) Green, M. L. H.; Saito, T.; Tanfield, P. J. *J. Chem. Soc. A* **1971**, 152.

bisphosphine−Ni complex, the corresponding barriers are too high to make N−H bond cleavage feasible. The large energy required to transfer one hydrogen from N to Ni can be partially ascribed to the fact that the H atom is forced to get out of the plane during the transfer. The temporary loss of coplanarity at the $N{=}CH_2$ fragment, together with the complete loss of π-interaction as the final product emerges, makes hydride formation a difficult process. On the contrary, the pathway leading to C−N cleavage involves less energy demanding rearrangements and is globally smoother (path **B** in Figure 4). After the branch point (**2a** or **3a**), the preference is clear; kinetic factors are mainly responsible for the observed selectivity of C−N (Figure 4) over N−H (Figure 6) bond activation.

IV. Conclusions

The main conclusions drawn from the current study can be summarized as follows.

(1) The actual active catalyst in the oxidative addition of ammonium and iminium salts is found to be the bisphosphine−nickel complex. Other ligands in the reactant species (N_2, CO_2) do not take part in the reaction.

(2) The reaction of allylammonium salts with Ni(0) complexes is found to proceed via an associative mechanism, path **B**, involving (i) coordination of the allylammonium cation to the active metal catalyst, (ii) activation of the C−N bond leading to the bis(phosphine)(π-allyl)Ni complex **1d**, and (iii) recoordination of the NH_3 followed loss of a phosphine ligand.

(3) On the other hand, the analogous reaction involving allyliminium salts prefers a dissociative mechanism, path **A**, involving (i) coordination of an allyliminium cation to a transition metal complex, (ii) dissociative of one of the phosphine ligands, followed by activation of C−N bond, leading to the monophosphine−nickel product.

(4) The preference of the C−N over N−H bond activation is a result of kinetic factors; the N−H bond activation process requires a much larger energy barrier than the C−N activation one.

Acknowledgment. The use of the computational facilities and programs at the Emerson Center (Emory University) is acknowledged. The present research is in part supported by a grant from the National Science Foundation (Grant No. CHE-9627775) and by DGES Project No. PB95-0762. M.T. expresses her gratitude to the Generalitat de Catalunya for financial help through CIRIT Project No. FI/94-5001 and to the Institute of Computational Chemistry (University of Girona) for additional allocation of computer time.

Supporting Information Available: Table S-1: The ONIOM total and relative energies of intermediates **2b** and transition states **TS(2b→2)** for the real system. Scheme S-1, Figure S-1: complementary to Figure 3. Figure S-2: complementary to Figure 4. Figure S-3: complementary to Figure 6. Figure S-4: complementary to Figure 5. This material is available free of charge via the Internet at http://pubs.acs.org.

OM000468A